INITIAL CHARACTERIZATION OF COHERENT SYNCHROTRON RADIATION EFFECTS IN THE APS BUNCH COMPRESSOR[*]

M. Borland[†] and J. Lewellen, Advanced Photon Source, Argonne National Laboratory, Argonne, IL

Abstract

A chicane bunch compressor was recently installed in the Advanced Photon Source (APS) linac in support of the Low-Energy Undulator Test Line (LEUTL) free-electron laser (FEL) project. As in any magnetic compression system, the use of bending magnets raises concerns about corruption of the emittance by coherent synchrotron radiation (CSR). In this paper, we present results of an initial characterization of these effects in the APS system. We also compare the measurements to simulations with the program `elegant`. The horizontally bending compressor is equipped with numerous diagnostics to aid in the exploration and reduction of CSR effects. These include: a flag in the chicane center for imaging the energy distribution; a flag for critical beam size tuning at the exit of the final chicane dipole; a vertical-bending spectrometer line downstream of the chicane with two flags for imaging CSR-induced correlations between horizontal and energy coordinates; and a three-flag emittance measurement system downstream of the chicane.

1 INTRODUCTION

Fig. 1 shows a schematic of the APS linac [1] and bunch compressor. The linac comprises several Stanford Linac Accelerator Center (SLAC)-type 3-m, S-band structures. A photoinjector (PI) — consisting of a Brookhaven National Laboratory (BNL)-type photocathode electron gun and a single S-band structure — delivers a beam of 30 to 40 MeV with 0.2 to 0.3 nC per bunch at 6 Hz. Following the PI, a single klystron drives four S-band structures, providing typical beam energy of 150 MeV. These structures are followed by the bunch compressor chicane and are used to impart the energy chirp required for bunch compression.

The bunch compressor [2] consists of four identical dipoles. The first and second dipole are on a single power supply, as are the third and fourth. This arrangement supports an unusual feature of the chicane; namely, the ability to move the fourth dipole longitudinally in order to vary the symmetry of the chicane. Although this feature is presently unavailable because of design issues with the flexible vacuum chambers, simulations [3] indicate that the asymmetric chicane should exhibit less emittance growth than a symmetric chicane with the same R_{56}.

The bunch compressor area is well supplied with diagnostics. At the center of the compressor is a beam position monitor [4] (BPM) and a beam-imaging flag [5]. The former is used to control the beam energy, while the latter is used for imaging the incoming energy spectrum. Following the chicane are four quadrupoles, used for matching the beam into a three-screen emittance measurement system. There is also a vertically bending dipole beamline with a flag, used to measure the energy spectrum.

Next come two sets of four accelerating structures, each driven by a single, SLAC Energy Doubler (SLED)-ed klystron. For the studies reported here, these sections are phased for zero energy gain for bunch length measurement using the spectrometer after L5, as discussed below.
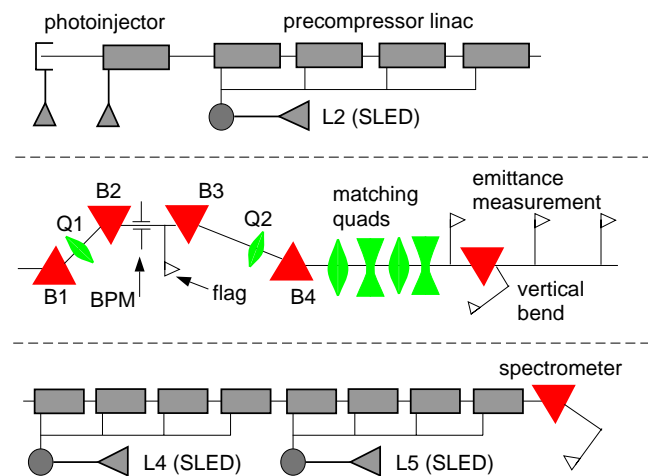
Figure 1: Schematic of APS linac and bunch compressor.

2 SIMULATION METHODS

Accurate knowledge of the longitudinal phase space of the beam entering the chicane is essential to meaningful prediction of the outcome of experiments. We used PARMELA for simulation of the PI, because this code includes space charge. Downstream of the PI, we use `elegant` [6], which does not include space charge but does include CSR [7]. For the design [3], we employed a nominal simulation of a 1-nC bunch and scaled the charge to the desired value for simulation with `elegant`, which is conservative because it overestimates the emittances. This simplifies the simulations in that we do not need to run PARMELA frequently. For the present work, we have continued this procedure. Future work will include more detailed simulation of the PI.

Several features of `elegant` made it the code of choice for this work. The program includes a fast algorithm for simulation of CSR effects [7], based on the 1-D formalism of Saldin et al. [8]. In brief, the dipoles are split into (typically) 100 pieces, with CSR kicks applied at the end of each piece. The CSR kicks are computed from the instantaneous longitudinal distribution at the end of the slice. The dipole itself is simulated using a symplectic integrator with exact energy dependence, so that the dispersion of the beam caused by the energy kicks is automatically included.

CSR in drift spaces is more important in our chicane than CSR in the dipoles themselves. `elegant` includes drift CSR using the assumption that the terminal CSR "wake" in the dipole propagates through the downstream drift spaces with no change in shape but with decreasing intensity [7]. The decrease is computed from the results of Saldin et al. [8] for a rectangular bunch.

`elegant` also includes exact simulation of rf curvature effects, which have an important influence on the dynamics when the beam is highly compressed. In addition, longitudinal and transverse wakes are included, as are nonlinear effects in transport through the dipoles.

`elegant` has a number of productivity-enhancing features that made it well suited to this work. Its use of the Self-Describing Data Sets (SDDS) file protocol [9] allows highly automated preparation and post-processing of input and output. Use of the SDDS file protocol has also enabled start-to-end simulation of FELs and their linac drivers [10].

3 EXPERIMENTAL METHODS

Our goal in these studies was to characterize the impact of CSR on the beam energy spectrum and emittance, and to compare our experimental results with simulation. Because the chicane magnets are fixed in position, we cannot vary R_{56} in order to vary the bunch length. Instead, we vary the energy chirp by varying the phase of the precompressor linac, while changing the rf voltage to keep the beam energy constant in the chicane.

The emittances were measured directly following the chicane using the three-screen technique. We collected 30 collapsed beam profiles for each plane for each screen. (If the beam is stable, 10 beam profiles give a reproducibility of about 10% in the emittances.) After background subtraction, the true rms beam size was computed from each profile. Profiles were analyzed to allow automatic removal of aberrant data, as judged by abnormal intensity or missing lines, for example. Estimation of error bars was done using a Monte Carlo technique: the standard deviation of the beam size at each screen was computed. These and the mean beam sizes were then used as input to a Monte Carlo simulation of 100 measurements.

Bunch length measurement employed a screen following a dipole downstream of the L5 accelerator structures. If beam is sent through L5 at the zero-crossing of the rf, then the fractional energy spread after L5 is $\sigma_{\delta,\pm}^2 = \sigma_{\delta,i}^2 \pm 2\langle\delta_i\phi\rangle\frac{V}{E} + (\frac{V}{E})^2\langle\phi^2\rangle$, where $\sigma_{\delta,\pm}$ is the fractional energy spread for the 0/180 phase, $\sigma_{\delta,i}$ is the incoming fractional energy spread, ϕ is the phase relative to the bunch center, V is the rf voltage, and E is the beam energy. $\sigma_{\delta,i}$ is measured by setting $V = 0$. The rms bunch length (in units of radians) is then given by $\sqrt{((\sigma_{\delta,+}^2 + \sigma_{\delta,-}^2)/2 - \sigma_{\delta,i}^2)/(V/E)}$. The measurement of fractional energy spread is calibrated by adjusting the dipole strength slightly and observing the motion of the beam spot. Resolution effects are automatically subtracted. When the resolution limit is reached, the method returns 0. To improve results, we reduced the $\langle\delta_i\phi\rangle$ term by using L4 at zero phase.

For bunch length measurements, we collected 20 beam profiles. Because the signal-to-noise ratio was low for many of the profiles, we applied a spot-finding algorithm that eliminated spurious tails, allowing more reliable determination of the rms beam size. Following this step, only the central 50% of the rms sizes were retained for further analysis, helping to reduce the effects of rf jitter.

4 EXPERIMENTAL RESULTS AND COMPARISON TO SIMULATION

In this section, we report on a measurement of emittance, incoming energy spread, and bunch length vs. precompressor phase. The "incoming" energy spread is that inferred from the profiles on the flag at the center of the chicane. Strictly speaking, these profiles may be affected by CSR, but that effect should only come into play when the beam is overcompressed. In both the experiment and simulation, we show the "apparent" energy spread, which is computed from the total beam size without attempting to correct for the monoenergetic beam size, which is unknown.

Fig. 2 shows the measurement and simulation results for energy spread, bunch length, and horizontal emittance. Initially, we had very poor agreement between simulation and experiment for all three quantities. We used `elegant` with CSR turned off inside an optimization script to fit the observed bunch length by varying the rms longitudinal properties of a Gaussian beam. We then transformed the PARMELA-generated beam in order to give it the same rms properties, including the nominal rms emittances. Finally, we ran a phase-scan simulation with CSR, obtaining the data shown in Fig. 2. The close match of the energy spread data validates the matching of the input conditions.

The emittance growth is also reasonably close to the measurement, in particular in the appearance of a narrow spike in the emittance near full compression. This feature is always seen in our experiments, as is the slight bump and the increase in noise in the emittance in overcompression. On the decompression side, there is also a slight emittance bump, but this is believed to be an artifact resulting from adjustment of the camera aperture.

`elegant` predicts more growth, a slightly narrower emittance peak, and a different phase for maximum growth than was measured. One source of the differences is our lack of knowledge of the detailed longitudinal phase space. The
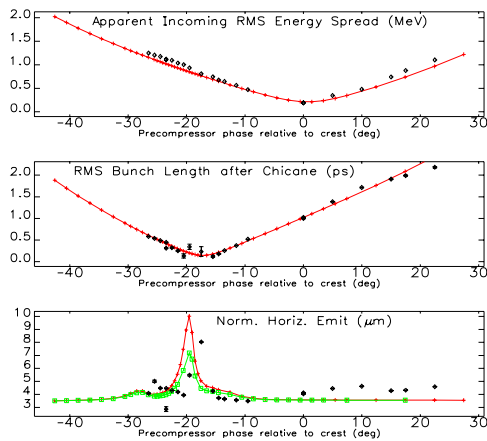
Figure 2: Comparison of experiment and simulation. The lower emittance curve used alternative binning and smoothing parameters (see text).

amount of the emittance growth and its phase of occurrence depends not only on the rms bunch length but on the severity and phase of occurrence of narrow spikes in the compressed temporal distribution. These spikes are related to the nonlinear relationship between phase and momentum in the beam from the PI [11].

Phase and timing jitter in our system is on the order of $1°$, hence the experimental results are averaged over about $1°$ of rf phase, which results in a broadening and diminishing of the emittance peak relative to the simulation.

Finally, changes in the simulation parameters can also alter the result. The above result was obtained by using 3,072 bins and a Savitzky-Golay smoothing filter with a half-width of six bins. Changing this to 512 bins and a smoothing half-width of one bin changes the peak emittance from 10 μm to 7 μm. The original binning and smoothing parameters were derived from tracking runs with up to 400,000 particles, and they are believed to be reliable. The use of the derivative of the longitudinal density in the Saldin formalism makes for sensitivity to the binning and smoothing parameters.

One feature that appears consistently in the data is an instability in the bunch length and energy spread near full compression. This feature is seen in the large error bars and poorly fit points in the bunch length near full compression. These values do not reproduce in the experiment. The variation is presumably caused by phase and timing jitter and pulse-to-pulse variation in the laser.

A second experiment involved measurement of energy spread at the center of the chicane and after the chicane, along with measurement of the bunch length. In this case, the fitting procedure described above did not return a stable result for the longitudinal twiss parameters, nor did it achieve a match to the incoming energy spread. Hence, we omit simulation results. The experimental data are shown in Fig. 3. Simulation with a nominal beam shows similar features, including the slight dip followed by an increase in

the final energy spread that occurs near full compression. We will repeat this experiment and report on the results in a future publication.

5 ACKNOWLEDGEMENTS
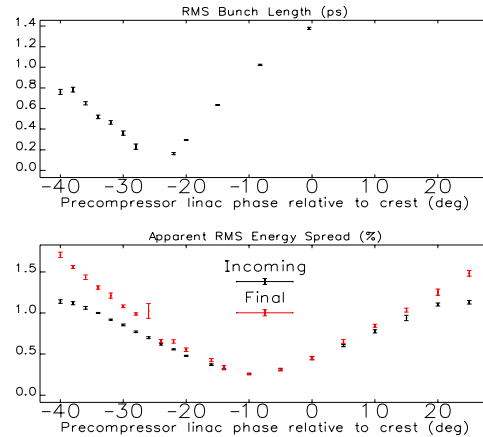
Figure 3: Measurement of the bunch length and incoming and final energy spread for 266 pC per pulse.

6 REFERENCES

[1] G. Travish et al., "High-Brightness Beams from A Light Source Injector," Proc. Linac 2000 (2000).

[2] M. Borland et al., "A Highly Flexible Bunch Compressor for the APS LEUTL FEL," Proc. Linac 2000 (2000).

[3] M. Borland, "Design and Performance Simulations of the Bunch Compressor for the APS LEUTL FEL," Proc. Linac 2000 (2000).

[4] R. Lill et al., "APS LEUTL Bunch Compressor Beam Position Monitor System," Proc. PAC 2001.

[5] B. Yang et al., "Design and Performance of a Compact Imaging System for the APS Linac Bunch Compressor," Proc. PAC 2001.

[6] M. Borland, APS LS-287, September 2000. http://www.aps.anl.gov/techpub/lsnotes/lsnotesTOC.html

[7] M. Borland, "Simple Method for Particle Tracking with Coherent Synchrotron Radiation," PRST-AB, to be published.

[8] E. L. Saldin et al., *NIM* A **398**, 373 (1997).

[9] M. Borland, Proc. PAC 1995, Dallas, Texas, pp. 2184-2186 (1996).

[10] M. Borland et al., "Start-to-End Jitter Simulations of the Linac Coherent Light Source," Proc. PAC 2001.

[11] M. Borland, "Design and Performance Simulations of the Bunch Compressor for the Advanced Photon Source's Low-Energy Undulator Test Line Free-Electron Laser," submitted to PRST-AB.